Underground Metal Pipeline Localization Using Low-cost Wireless Magnetic Sensors Mounted on an Excavator

Jeonghee Kim, *IEEE Member*, Youngjib Ham, and Hangue Park, *IEEE Member*

Abstract— **To minimize the excavation damage of underground pipelines, we propose to provide real-time feedback to operators by monitoring the distance information from the underground pipeline. Despite multiple efforts to locate underground ferromagnetic pipelines using the magnetic anomaly detection, it has not been implemented in real-time excavation operations due to low signal-to-noise ratios, unknown external magnetic interference, and high computational power. To address these limitations, we propose an approach to locating a custom-designed wireless sensor system on the excavator bucket to increase accuracy of real-time distance estimation with efficient external magnetic interference cancellation. We present the system using a 14:1 lab-scaled excavator and six sizes of ferromagnetic pipes. To create a distance estimation model of each pipe, we measure the magnetic anomaly caused by ferromagnetic pipes from eight distances (from 5 to 75 mm, spaced 10mm apart). The wireless system with the localization algorithm successfully estimates the distance between the sensor and the pipe with a less than 4.38±1.62mm error overall. This pilot study shows that the proposed system with the localization algorithm is able to accurately locate pipes. This will lay the foundation for providing accurate spatial information, and ultimately prevent critical excavation/drilling damage at construction sites.**

***Index Terms*—Distance estimation, external magnetic interference cancellation, ferromagnetic underground pipelines, magnetic anomaly detection.**

I. INTRODUCTION

DAMAGE to underground utilities (e.g., telecommunications, gas, TV, water, sewer) is a possibility on every excavation site [1] and can result in costly consequences such as disrupting essential services, downtime, and potentially serious injuries or death. Approximately 379,000 incidents of the underground utility damage were reported in the United States (U.S.) in 2016, an increase of 20% from 2015, and an additional cost of approximately $1.5 billion to society [2]. For example, it was reported that more than 50% of Atmos Energy's hazardous leaks in 2018 were caused by excavation damage [3]. Even minor damage, such as a scrape, dent, or crease in a pipeline or its coating, can weaken a pipeline and lead to a future leak. Therefore, an efficient method of detecting buried objects (i.e., pipelines) to prevent accidents at construction site is important not only to ensure a safer environment on construction sites but also to save unnecessary costs.

To minimize excavation/drilling damage on real construction sites, operators use caution while digging along with two main approaches: 1) the proper marking of underground pipelines reported to the Federal Communications Commission [4]-[6] and 2) radar-based scanning that detects pipelines [7]-[16]. These mitigation efforts, however, will not sufficiently reduce excavation damage to underground utilities. To address the limitations of these approaches, we must first understand why they are limited.

Marking pipelines: Some excavation damage can be prevented by contacting 811, the number that the Federal Communications Commission has designated as the national toll-free "Call Before You Dig" number in the U.S. [17]. An 811 representative will take information about planned excavation activities and notify the appropriate utility companies to locate and mark buried lines they own at the location specified in the call ticket. The call must be placed at least two to three business days before excavation begins to ensure that buried utility-owned pipelines are properly located and marked. Based on the types of the utilities, different color-coded markers would be provided for this purpose. Despite the benefits, this practice has not had a significant effect at reducing the number of incidents. Evidence of damage (particularly to telecommunication and television lines) has been increasingly reported in the U.S. [18]-[20], possibly the result of errors in the marker location or the provision of no depth information nor real-time feedback.

Manuscript received Month xx, 2xxx; revised Month xx, xxxx; accepted Month x, xxxx. This work was supported by the National Science Foundation Award 2026574.

J.H. Kim is with the Department of Engineering Technology and Industrial Distribution, Texas A&M University, College Station, TX 77843 USA (corresponding author; e-mail: jeonghee.kim@tamu.edu).

Y.J. Ham is with the Construction Science Department, Texas A&M University, College Station, TX 77843 USA (e-mail: yham@tamu.edu).

H. Park is with the Department of Electrical and Computer Engineering, Texas A&M University, College Station, TX 77843 USA (corresponding author; e-mail: hangue.park@tamu.edu).

Radar pipeline scanning: The radar-based pipeline scanning can be performed in dangerous/critical areas to prevent pipeline damage. Typically, handheld devices are used to scan the target area for construction sites. In the last several decades, advances in the field of remote sensing and visual augmentation (e.g., augmented reality, virtual reality) have enhanced the spatial awareness of buried utilities [21]-[26] by providing workers with more information (e.g., regarding depth) with more displays. Such advances have dramatically improved operator performance and mitigated the likelihood of accidents. For example, locating technology such as ground penetrating radar (GPR) enables operators to use three-dimensional underground utility mapping to obtain more precise (depth) information about buried utilities [7]-[26]. If such locating technology, along with GPS/GIS and augmented reality (AR), can be fully utilized before excavation work, the machine guidance system may provide operators with information of the proximity of the excavator bucket to 3D models of buried utilities [4],[6],[21]-[26]. Even though this GPR technology can provide an accurate spatial information for pipeline locations, it takes a substantial amount of time to scan and process the laser signals that detect the pipelines. Moreover, if the penetration distance of the device (radar) is limited, it may not be capable of detecting all pipelines from ground level.

It is also critical to understand the main causes of underground utility damage. The most common causes are insufficient excavation practices and insufficient location practices. Even if utilities are located and marked, and depth information is known prior to excavation, the current control interface of an excavator is not intuitive enough to accurately control an excavator arm. Therefore, efficient feedback to convey depth information to an excavation operator on the construction site is another important issue [27].

At the same time, to provide the operator with reliable information, we need to be able to estimate the depth information of buried pipelines in real time. However, providing accurate and reliable spatial information for the underground environment has been a challenging task, because sensors (e.g., vision, distance, depth) are usually designed for the overground localization [28]-[32], and cannot detect the objects at the underground environment. To monitor spatial information in underground environments, several studies have proposed using inertial measurement units (IMUs) with noise reduction algorithms, and they have applied them to various underground localization tasks for construction activities such as excavation and drilling [33]-[38]. Specifically, the magnetometer, among the IMU sensors, plays an important role in underground environment as it can monitor the magnetic anomaly from the buried metal objects. As metal-based pipes (i.e., ferromagnetic object) deform the earth's magnetic fields (EMF) near the pipelines, the distorted magnetic field can be utilized to estimate the location of the metal-based pipes (see Fig. 1). Note that, the most of the materials covering the ground are transparent to the magnetic fields, except for the particular soils that contain magnetism [39], [40]; so if we can efficiently eliminate the magnetic interference, including the EMF and external magnetic fields (i.e., magnetic soil), then the metal-based pipes can be effectively localized. By monitoring underground metal-based pipes using a magnetometer in real time, we can ultimately provide proper and intuitive feedback to the operators to avoid any accident via a visual, auditory, or tactile channel.

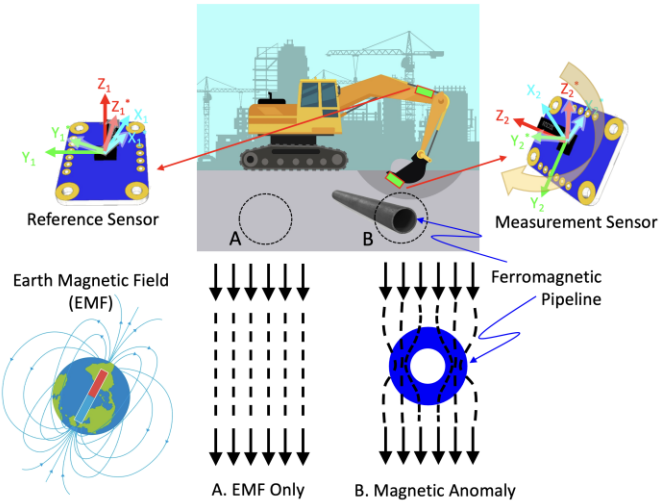

Fig. 1. Overview of the Real-time ferromagnetic Pipeline Detection System (RPDS) that utilizes Magnetic Anomaly Detection (MAD) to locate the hidden underground ferromagnetic objects with external magnetic interference (EMI) cancellation.

Several research groups have worked on magnetic anomaly detection (MAD) for underground pipeline localization, on the purpose of moving ferromagnetic objects or drilling activities [41]-[44]. The most common method of distance or depth estimation for the underground ferromagnetic pipelines is magnetic dipole reconstruction (MDR) [45]-[53]. The MDR approach, as a forward modelling, can accurately do the magnetic anomaly detection (MAD) of target pipelines and model the magnetic dipole to estimate the depth from the ground. To increase the accuracy of MDR, several studies have implemented novel algorithms to increase signal-to-noise ratio, such as stochastic resonance [47] and deep learning neural networks [48]. They have evaluated their approaches with mathematical simulation models and measurement outcomes to show how much the signal-to-noise ratio can be improved.

Moreover, the MDR approach requires a high computational power to estimate the distance [49]-[51]. Others have explored different scheme to reduce its computational power, such as segmentation strategy and section segmentation method approach. However, they reported the time for calculation as tens or thousands of seconds [51]. Other studies have demonstrated the application of MAD in operations of placing the sensor in stationary positions or directional movements (e.g., horizontal drill movements). A few of them estimated the distance between the magnetic sensors and target ferromagnetic objects, yet the distance range (e.g., several meters) did not cover the interested distance to be implemented in excavator movements. Moreover, none of them tested the system in actual excavation movements to estimate the distance from the pipes.

To minimize an excavation damage of the underground pipeline, our approach is to provide real-time feedback (e.g., auditory, visual, vibro- or electro-tactile [54], [55]) to the

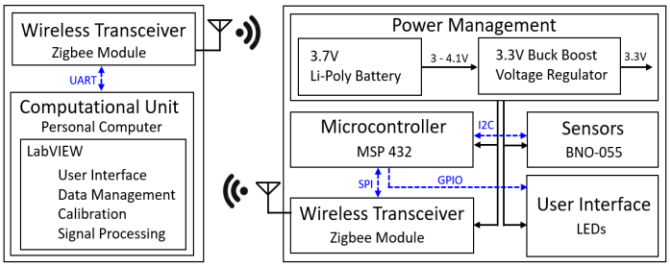

Fig. 2. Block diagram of the wireless multi-sensor recording hardware of the Real-time Pipeline Detection System (RPDS).

TABLE I
SPECIFICATIONS OF RPDS HARDWARE

Specification	Value
Control Unit	
Microcontroller Unit	MSP432
Wireless Module	Xbee 2.4GHz RF Module
Control Unit Dimensions	40 x 55 mm^2
Power Source	3.7 V 2000 mAh Li-ion polymer battery
Board Weight (with Battery)	22 grams (60 gram)
Sampling Rate	20 Hz
Inertial Measurement Unit (IMU) Modules	
Sensors	BNO-055
Sensor Unit Dimensions	20 x 27 mm^2
Sensor Unit Weight	3 gram per each module
Accelerometer	±16g
Gyroscope	±2000°/s
Magnetometer	±1300μT (x-, y-axis), ±2500μT (z-axis)
Magnetic Field Resolution	~0.3μT
Operating Hours	~ 20 Hours

operators based on the distance information of the underground ferromagnetic pipeline. Considering the speed of excavator arms (e.g., boom and stick) or bucket, this approach requires to estimate the near field proximity information (e.g., up to 1x or 2x of bucket height) in subsecond scale during excavation motions. Any of the existing approaches cannot be employed because they cannot estimate the distance within the subsecond time window. Further, existing approaches did not function at the distance range of our interests, were not tested in multi-degree movements, and did not consider external magnetic interferences of equipment body (i.e., excavator).

To accurately estimate the proximity information within this scope, we propose an approach to locate the sensor at the tip of the bucket. As the excavation proceeds, the sensor can get close to the underground pipeline, so it can increase the signal-to-noise ratio. At the same time, we can increase a control resolution because the tip of the bucket is the main collision point. However, it might be challenging because the excavator body, boom, stick, and buckets are also composed of ferromagnetic materials; and therefore, an external magnetic interference should be efficiently removed. Moreover, the earth magnetic fields need to be cancelled too while the sensors are moved along with the multi-degree excavation motions.

To efficiently remove the external magnetic interference, several prior studies have employed a reference sensor at a distance to efficiently distinguish the target MAD while cancelling the common mode interference [52], [53]. However, this is not applicable to the case where the two sensors are on the different ferromagnetic materials in movement. Therefore, we selected the linear relationship between the reference and

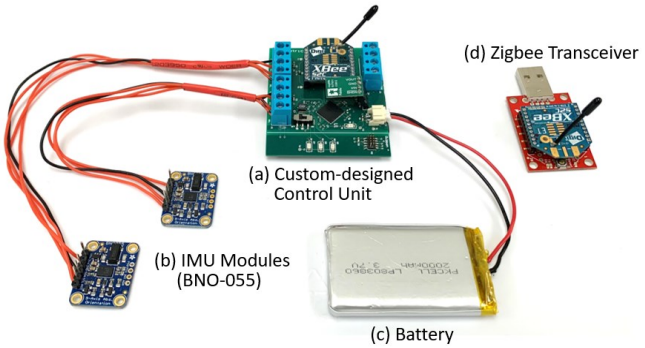

Fig. 3. Actual wireless multi-sensor recording hardware of the RPDS: (a) a custom-designed control unit, (b) inertial-measurement unit (IMU) modules, (c) a Li-poly rechargeable battery, and (d) a Zigbee wireless transceiver.

measurement sensors, with the static external magnetic interference for each sensor. The virtual linear relationship based on the measurement data was utilized to cancel the external magnetic interference (EMI). Note that any dynamic external magnetic interference cannot be cancelled and the ferromagnetic pipeline can be easily detected. This approach had been applied to the magnetic localization for magnet-based tongue-controlled assistive technology and its efficacy was demonstrated with multiple system-level operation tests [56]-[60].

Therefore, we propose the *Real-time Pipeline Detection System (RPDS)*, which employs a pair of magnetic sensors and a localization algorithm to detect magnetic deformation caused by ferromagnetic pipes as a bucket of the model excavator approaches the target ferrogmagnetic object during the actual excavation movement. To accurately estimate the distance/depth from a pipeline, we must first increase the signal-to-noise ratio by eliminating external magnetic interference. The main source of magnetic interference is the EMF and environmental magn etic fields (i.e., magnetic soil), which is relatively easy to eliminate since they are considered a common mode noise. Another source of interference is magnetic deformation caused by the excavator body (i.e., bucket, the stick, and the boom), which typically consists of ferromagnetic material. To closely collect the magnetic deformation from the pipes, our system requires that the measurement sensor be located at the teeth of the excavator bucket, which means that the sensor will continuously move along with the bucket during excavation movements. To address the challenges of constantly moving sensor(s) for the real-time monitoring of underground pipes, a specialized signal-processing procedure requires to efficiently eliminate magnetic interference using a reference sensor during the excavation movements. Moreover, the proposed localization algorithm should accurately estimate the distance from the measurement of the magnetic anomaly caused by the ferromagnetic pipes.

In this study, we developed the RPDS and evaluated the system with pipes of various diameters and distance, and a set of experimental results showed that the RPDS can effectively eliminate magnetic interference and accurately estimate the

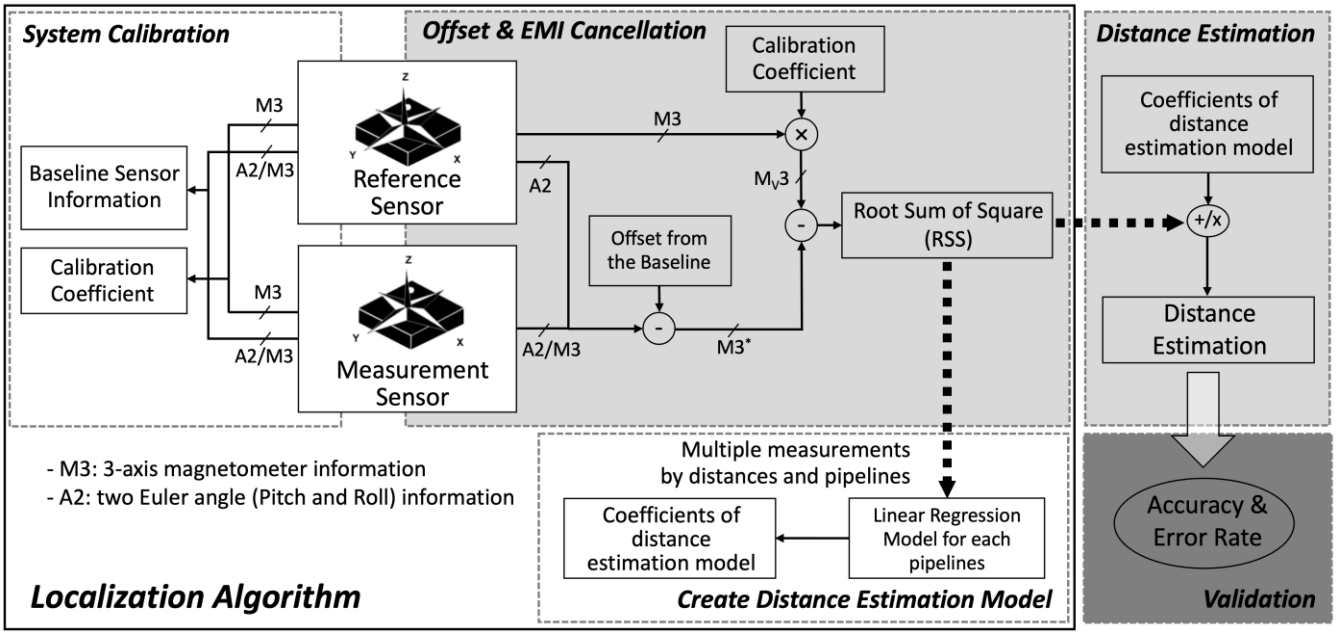

Fig. 4. Block diagram of the RPDS localization algorithm including calibration, sensor offset and external magnetic interference cancellation, creating the distance estimation models for each pipe, and the actual distance estimation. For the system validation, we analyzed the error rate from the difference between the actual distance estimation from the distance estimation model and its reference distance.

distance from the ferromagnetic pipes. The proposed RPDS system can complement existing excavation tools, and will ultimately support operators in their efforts to protect underground utilities during excavation activities that require more caution by providing an accurate spatial information.

II. Methods

The RPDS consists of wireless multi-sensor recording hardware with a localization algorithm including offset and magnetic interference cancellation (calibration) and distance estimation.

A. Wireless Multi-sensor Recording Hardware

The wireless multi-sensor recording hardware of RPDS consists of a custom-designed control unit with two IMU modules, a Li-poly rechargeable battery, a wireless transceiver, and a laptop computer. The hardware collects multi-dimensional sensor data and conveys information to the computer, which processes the sensor information. The transceiver takes charge of the wireless data communication. The laptop computer provides the user interface and processes the pre-built localization algorithm to eliminate offset and external magnetic interference and to determine the distance from ferromagnetic pipes. The overall block diagram of the hardware of RPDS is illustrated in Fig. 2, and the system specifications are summarized in Table I. The RPDS firmware was programmed using the Texas Instrument Real-Time Operating System (TI-RTOS) MSP432 package. The hardware system, sensor modules, and the transceiver with the USB data conversion module are shown in Fig. 3.

The custom-designed hardware of RPDS consists of a microcontroller (MCU; MSP432, Texas Instruments, TX USA), a power-management circuit, a Zigbee wireless transceiver module (Xbee 2.4GHz RF Module; Digi International, MN USA), and two IMUs (BNO-055, Bosch Sensortec, Germany). The IMU sensor data is delivered to the MCU via a serial communication protocol (I^2C), and the MCU creates a data package to transmit it via the Zigbee wireless protocol. The power-management circuit converts the battery input to a 3.3 V regulated supply to power all electronic components.

The IMU module, BNO-055, provides the output of the accelerometer, the gyroscope, and the magnetometer as well as three-dimensional Euler angle information as outputs of the data fusion mode using the IMU data. The information is used as reference angle for the excavator boom and the bucket. The main signal processing algorithm, however, uses the three-axis magnetometer information. To collect accurate Euler angle output (i.e., the pitch, the roll, and yaw within ±3 degrees) using their own data fusion algorithm, each sensor module must undergo the sensor calibration process [61].

B. Offset and External Magnetic Interference Cancellation

The localization algorithm of the RPDS consists of an increase in the signal-to-noise ratio and an estimate of the distance. To accurately locate ferromagnetic pipes using the magnetic sensors, we increased the signal-to-noise ratio by following two major steps: (1) offset and (2) external magnetic interference (EMI) cancellation. A flowchart of the localization (sensor signal processing) algorithm that both eliminates offset and common-mode EMI and estimates distance from the pipe is shown in Fig. 4.

We began by removing offsets, defined as any deviation from the baseline sensor information at the initial excavator location, referred to as *Offset cancellation*. Offset occurs when magnetic sensors are very close to extremely high magnetic fields, mainly caused by magnetic hysteresis. Since both sensor modules can provide Euler angle information used to identify a

baseline location at the initial stage, we compared the sensor values to the baseline sensor values when the excavator was positioned at the initial stage. If the system detected a certain level of offset in the measurement sensor from the baseline sensor information, it automatically subtracted the offset.

After eliminating the sensor offset, we applied *EMI cancellation*. Magnetometers detect changes in the magnetic field from not only the ferromagnetic pipes but also the EMI, such as the EMF and external ferromagnetic objects (i.e., parts of the excavator body, magnetic soil). The EMI, however, can degrade the performance of the distance estimation of localization algorithm because the EMI can be a significant noise for the MAD measurement caused by the ferromagnetic pipes. Thus, EMI cancellation is important, enhancing the performance of algorithm that determines the distance between the sensor and the ferromagnetic pipes.

The core of EMI cancellation is subtracting the real-time EMI using a reference sensor (located at the top of the boom) to the measurement sensor (located at the tip of the excavator bucket) [52], [53]. Since the two sensors are not pointed in the same direction, they must be virtually aligned in parallel [56]-[60], [62], [63]. Then the magnetic fields of the reference sensor (EMI) are subtracted from those of the measurement sensor. As a result of subtraction with virtual alignment, the common-mode components of the magnetic sensor output, mainly the result of the EMI, are cancelled out while the differential-mode components resulting from the ferromagnetic pipelines are retained.

To virtually align both sensors in parallel, we first collected sensor information with possible common-mode noise from the EMI while executing possible excavation movements, maintain the relative sensor locations constantly without any pipes. We refer to this procedure as *system calibration*. Once we collected the sensor data from this calibration procedure, we calculated the calibration coefficients that could be used for virtual alignment of the sensor modules. During the calibration procedure, we also collected baseline sensor information (i.e., magnetic sensor data and Euler angle information) for both sensors at the initial position of the stick, the boom, and the bucket of the excavator (Fig. 5a) to detect and cancel the offset.

The outputs of the three-axis magnetometer from the measurement sensor (M), located at the tip of the bucket, are X_M, Y_M, and Z_M and those from the reference sensor (R), located at the top of the stick, are X_R, Y_R, and Z_R. After we collected the magnetic sensor information during system calibration, we calculated the calibration coefficients of the linear relationship between the reference and measurement sensors. The linear relationship between the original (X_R, Y_R, Z_R) and the virtually rotated modules (X_{VR}, Y_{VR}, Z_{VR}) can be expressed in Eq. (1):

$$\begin{cases} X_{VR} = a_x X_R + b_x Y_R + c_x Z_R + d_x \\ Y_{VR} = a_y X_R + b_y Y_R + c_y Z_R + d_y \\ Z_{VR} = a_z X_R + b_z Y_R + c_z Z_R + d_z \end{cases} \quad (1)$$

where a, b, c, and d are linear coefficients, indicating the relative orientation of the two sensors. These coefficients were found using the multilinear regression algorithm during the calibration procedure with the presence of EMI, yet without any ferromagnetic pipes. After we virtually rotated the reference sensor using the calibration coefficients from the calibration data, we subtracted the rotated reference sensor data from the measurement sensor data in Eq. (2).

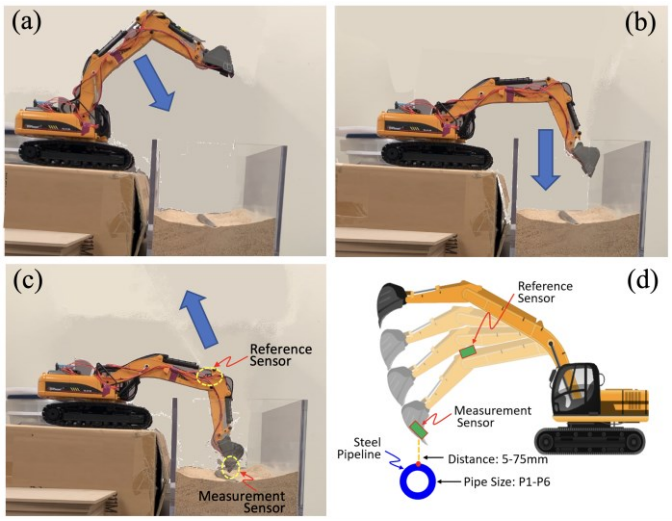

Fig. 5. Experimental setup to emulate the construction site using 14:1 scaled metal excavator model. The series of excavation movements for the distance estimation: (a)-(b)-(c)-(a) as a trial. (d) The nearest distance between the sensor and the pipeline was applied to estimate the distance from the data collection.

$$\begin{cases} X_{M^*} = X_M - X_{VR} \\ Y_{M^*} = Y_M - Y_{VR} \\ Z_{M^*} = Z_M - Z_{VR} \end{cases} \quad (2)$$

Thus, the output of measurement sensor subtraction with virtual alignment (X_{M^*}, Y_{M^*} ,Z_{M^*}) would be sensitive enough to detect changes in magnetic fields caused by the ferromagnetic pipes, yet insensitive to the EMI even while both sensors are in motion. We calculated the root sum of square (RSS; Eq. (3)) values of the offset and EMI free sensor information to create the distance estimation models. This output was also used for validation.

$$M^*_{RSS} = \sqrt{X_{M^*} + Y_{M^*} + Z_{M^*}} \quad (3)$$

C. Distance Estimation

To create a distance estimation model for each pipe, we first measured magnetic fields of various distances between the sensor and different sizes of pipes. From the RSS output of the measurement sensor of the various distances, we created a first-order linear regression model of each pipe for the distance estimation. The coefficient of the first-order linear regression model is expressed in Eq. (4):

$$y = a\,x + b \quad (4)$$

where x is the reference distance between the sensor and the pipes, and y is the RSS of magnetic fields. The linear regression models were created by the measurement of 10 trials at each of eight distances between 5 and 75 mm (for a total of 80 measurements per pipe). Once we created the distance estimation models, we reversely applied the actual measurements to estimate distances. We evaluated the distance

estimation algorithm by comparing the estimated distance to the reference distance.

III. Evaluation

The goal of this study is to evaluate how accurately the RPDS estimates the distance between the sensor and the pipe. This evaluation was performed by a 14:1 scaled metal excavator model that emulates the excavation operation at a construction site.

A. Experimental Setup and System Calibration

Figs. 5a -c show the flow of the excavator operation for each trial (from Figs. 5 (a)-(b)-(c)-(a) per trial) to estimate the distance between the measurement sensor (installed inside of the bucket teeth) and the pipe, based on the magnetic field measurements (RSS output). We used the data at the location of Fig. 5c for the validation. We manually changed the location of each metal pipe at eight distances spaced 10 mm apart: the closest was 5 mm and the farthest was 75mm (see Fig. 5d). At each distance, we conducted 10 trials (a full excavation movement), and used six different pipes for all measurements. Detailed pipeline specifications are summarized in Table II. We performed the experiment on a 14:1 lab-scaled metal excavator (Top Race TR-211M).

We first performed "sensor calibration" to implement the data fusion mode of the sensors to get accurate reference angular information before we mounted them on the excavator. We individually rotated th e sensor modules by changing them 45 degrees in all direction. This sensor calibration, which differs from the system calibration for offset and EMI cancellation, took about 30 seconds per sensor module. We then placed the sensors in two positions on the excavator: the teeth of the bucket and the top of the boom, and performed the system calibration. For the system calibration, we collected sensor data without any pipes, yet moved the boom of the excavator a s similar so that it resembled the natural excavation operation (repeated five times). We used the data to calculate the coefficients of the linear relationship model (Eq. (1)) for EMI cancellation and to collect the baseline sensor and angular information at the initial excavator position. To create the distance estimation models and estimate the actual distance, we used the calibration coefficients and the initial information from the system calibration that were saved in a text file.

TABLE II
Specifications of Pipelines

Index	Nominal Size	Diameter External (Inches)	Wall Width (Inches)	Weight Per Foot (Pounds)	Length (Inches)
P1	1.000	1.315	0.133	1.678	18.00
P2	2.000	2.375	0.154	3.652	18.00
P3	4.000	3.500	0.216	7.575	18.00
P4	4.000	4.500	0.237	10.79	18.00
P5	5.000	5.563	0.258	14.62	18.00
P6	6.000	6.625	0.280	18.97	18.00

All sample pipes are Structural Steel Pipe ASTM A500.
Mechanical Properties: Tensile = 58,000 and Yield = ±46,000.

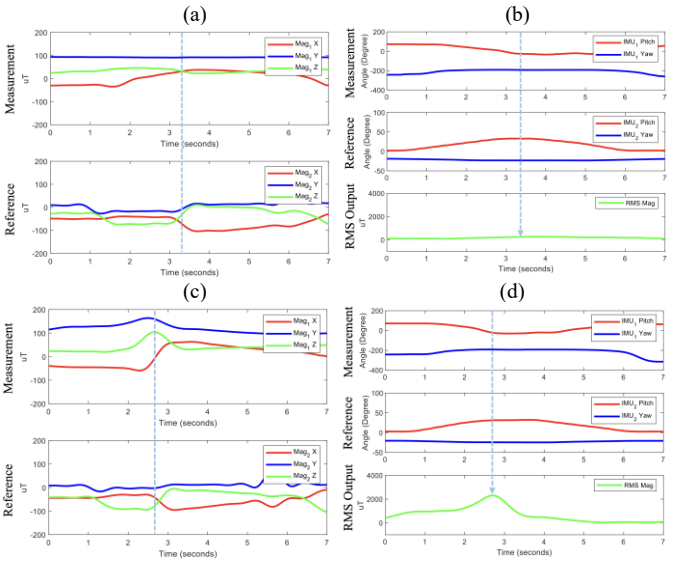

Fig. 6. Example graphs of magnetic field changes with and without pipes. Raw magnetic sensor outputs from both measurement and reference sensors (a) without pipes and (c) with the P2 pipe at 15mm distance. The Euler angle and the RSS output after the offset and EMI cancellation from the reference and measurement sensors (b) without pipes and (d) with the P2 pipe.

B. Distance Estimation Model and Validation

To evaluate the RPDS, we manually set the location of the pipes for the sensor data collection (1) to create the distance estimation model and (2) to estimate the distance between the sensor module and the pipe. After offset and EMI cancellation, we calculated the RSS of the magnetic sensor data for creating the distance estimation model for each pipe and validating the distance estimation.

We selected one of the six pipes and measured the magnetic fields of the eight distances ten times. The number of measurements for each pipe was 80 (10 times for the eight distances). As the average measurement of the RSS of the magnetic fields for each distance was correlated with the distance (see Fig. 7), we fit the linear regression model from the multiple measurements. We repeated the same procedure for six pipes (the number of measurements for the six pipes was 480). Then we obtained the raw sensor, pitch, and roll data, the RSS magnetic fields, and the coefficients of the linear relationships for distance estimation, which would be used to estimate actual distances.

After we created the distance estimation models for each pipe, we evaluated the accuracy of the distance estimation by comparing the difference between the estimated distances and the reference distances. We first selected one of the six pipes in a random order, and randomly measured one of the eight distances. Once we selected a distance, we repeated the excavation operation 10 times to estimate the distance. Once we completed the measurement with the eight distances, we randomly selected another pipe and repeated the same procedure. We estimated the distance using the offset- and EMI-free RSS output at certain locations (Fig. 5c), which we referred to the Euler angle information to find.

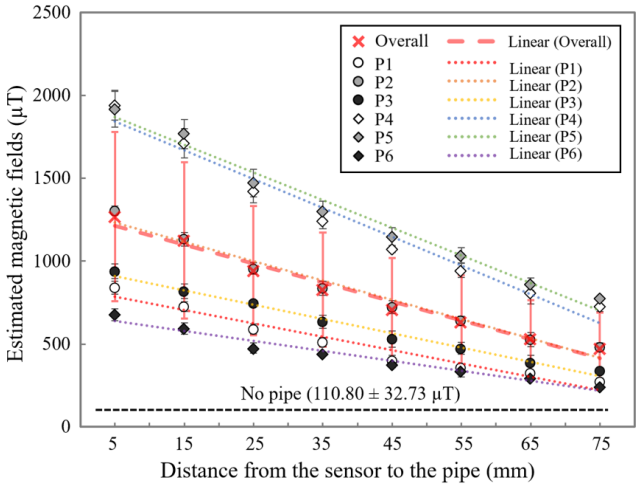

Fig. 7. Linear regression models for the estimation of the distance from individual and all pipes based on the RSS output from the pre-collected data. The bottom dashed black line represents the output without pipes.

TABLE III
COEFFICIENTS OF THE LINEAR REGRESSION MODEL FOR EACH PIPE

Index of Pipe	a	b	R^2
P1	-8.065	825.512	0.954
P2	-11.683	1292.486	0.978
P3	-8.657	954.755	0.989
P4	-17.376	1928.450	0.969
P5	-16.655	1951.175	0.980
P6	-6.125	676.352	0.978
Overall	-11.417	1271.400	0.977

y=ax+b; x: reference distance, y: RSS of measurement sensors

IV. RESULTS

Figs. 6a and 6c show the raw three-axis sensor data, and Figs. 6b and 6d show pitch and roll angle data and the RSS magnetic fields after offset and EMI cancellation for a single excavation movement with (Figs. 6c-d) and without (Figs. 6a-b) a two-inch diameter pipe (P2) at a distance of 15 mm.

The pitch and roll values of the closest distance between the sensor and the pipe during one excavation movement, as in Figs. 6b and 6d, was 31 and -24 degrees for the reference sensor, and -24 and -191 degrees for the measurement sensor at the position in Fig. 5c. Displaying a summary of overall data collection, Fig. 7 presents the RSS magnetic fields of the eight distances (from 5 mm to 75 mm) between the tip of the bucket (measurement sensor) and the pipe for various diameters of pipes (P1-P6). Fig. 7 displays the average and standard deviation from the data collection of each of the distances and each pipe (n=10 for each point). From the collected data, we obtained the linear regression model for e ach pipe and found that all linear regression models for d istance estimation for the six pipes fit the data collection well and showed a greate r than 0.95 coefficient of determina tion (R^2). A summary of the coefficients of each linear regression model and their R^2 values were summarized in Table III.

Applying the linear regression model, we reversely fed the coefficients to estimate the distance from th e RSS magnetic fields. A summary of the estimated distances from the data collection were summarized in Table IV. The summary of the data was from ten repetitive validation measurements (n=10) for each distance and each pipe; the overall data was a summary of averaged data for six pipes at each distance point. The overall error rate for the distance estimation using the RPDS was about 25%. Even though the error rate was higher for the closer distance (about 123% at a distance of 5 mm), the average difference between the distances was less than 5 mm for all sizes of pipes. When we focused only on the error rate for the distance higher than 35mm, the error rate was decrased by about 7.77%.

V. DISCUSSION

The coefficients of the distance estimation model did not show a strong relationship according to the size of the pipe (diameter), but it showed well-fitted linear regression models (R^2 higher than 0.95) for all pipes. Once we know the characteristics of the pipes (e.g., diameter, material, width, direction), we can estimate the distance between the pipe and the sensor with less than a 5 mm error for all cases except for the shortest distance (5 mm). If we have no information about the pipe and applied a generalized distance estimation model, then the error rate can be significantly increased (~790.09% for 5mm; ~44.67% for the distance higher than 35mm, which is 5.75 times worse). However, the characterization of the

TABLE IV
DISTANCE ESTIMATION OUTPUTS FROM THE EXCAVATION MOVEMENTS

Index of Pipe	Estimated distance between the sensor and pipes (mm)							
	5	15	25	35	45	55	65	75
P1	-1.76 ± 4.79	12.47 ± 3.72	29.23 ± 3.71	39.03 ± 3.43	52.48 ± 3.51	57.98 ± 1.67	61.86 ± 1.85	68.72 ± 2.94
P2	-0.99 ± 2.34	13.77 ± 3.58	28.89 ± 2.92	39.08 ± 3.66	48.81 ± 3.46	55.78 ± 2.37	65.56 ± 3.64	69.10 ± 1.97
P3	1.93 ± 5.10	15.67 ± 5.01	24.10 ± 2.16	37.00 ± 4.38	49.10 ± 5.75	55.44 ± 4.02	65.74 ± 5.18	71.00 ± 2.00
P4	-0.65 ± 5.17	12.48 ± 5.06	29.34 ± 3.74	39.36 ± 2.84	49.25 ± 1.28	56.62 ± 2.42	64.58 ± 3.80	69.03 ± 1.89
P5	2.00 ± 5.86	11.03 ± 5.30	28.80 ± 5.05	38.91 ± 3.57	48.27 ± 3.35	54.97 ± 2.66	65.43 ± 2.26	70.59 ± 1.54
P6	-1.28 ± 6.01	13.01 ± 4.81	28.18 ± 7.10	38.05 ± 2.03	48.78 ± 3.03	55.71 ± 5.12	62.70 ± 1.46	71.28 ± 2.36
Overall	-0.13 ± 1.66	13.01 ± 1.57	28.09 ± 1.99	38.57 ± 0.89	49.45 ± 1.52	56.09 ± 1.07	64.31 ± 1.64	69.96 ± 1.13
Estimated Distance Difference	6.19 ± 1.13	3.94 ± 0.85	4.46 ± 1.69	4.19 ± 0.61	4.90 ± 1.15	3.69 ± 2.53	2.67 ± 0.60	5.04 ± 1.13
Error Rate (%)	123.72 ± 22.61	26.26 ± 5.69	17.83 ± 6.74	11.98 ± 1.75	10.89 ± 3.35	5.14 ± 1.64	4.11 ± 0.92	6.72 ± 1.51

Overall error rate: 25.83 ± 38.87 %; overall difference between the measurement sensor and the pipe: 4.38 ± 1.62 mm;

magnetic fields around the ferromagnetic pipe will improve the generalized distance estimation algorithm without information about the pipe. For example, the magnetic field change rate, which depends on the size of pipes, can be applied to estimate the size of the pipes. Moreover, we can apply signal processing schemes such as principal component analysis and machine learning classifiers to improve the generalized distance estimation. In our future work, we will develop a generalized solution with or without prior knowledge of pipe sizes.

From preliminary measurements, we found that some offset caused by magnetic hysteresis in the sensor measurements accumulated over the time. Offset was observed by the magnetometer, particularly when the sensor was close to high magnetic fields (i.e., a ferromagnetic pipe), degrading the distance estimation. Therefore, we collected the baseline sensor data during the calibration at the greatest distance between the sensor and the pipe, initial position of the excavator (see Fig. 5a). Based on the Euler angle of both measurement and reference sensors, we could find the initial position of the sensors. Thus, we were able to eliminate the offsets by locating the initial excavator position and subtracting the offset by comparing measurement sensor output with the baseline sensor values; estimated the distance with the high accuracy distance.

To evaluate the feasibility of estimating the distance to a moving object, we compared the measurement and reference distance values offline. We took all measurements with a metal-based model excavator at the lab-based testbed, which resembles a real construction site. We also simulated possible EMI caused by the excavator body and soil, and potential ferromagnetic objects (i.e., metal pipes). To change the distance between the sensor and the pipe, however, the current setup of the evaluation experiment changed only the angle of the boom; that is, the relative position/angle between the reference and measurement sensors was constant, which is an unrealistic condition in real excavation movement. However, we expect to be able to position both measurement and reference sensors on the bucket—one at the tip of the bucket and the other at the connection to the stick—by replicating the setup used in this study. If we are able to do so, the excavator bucket will freely move in any direction by changing the boom and stick angles, even though the relative position of both sensors will remain the same. Moreover, the standard size of the excavator bucket, between 24 and 48 inches, should ensure that the measurement and reference sensors are sufficiently far from the bucket to be utilized this signal processing algorithm.

The current RPDS system has two sensor modules connected via wires, which may not be suitable for the rough construction environment. We plan to develop a fully wireless system with individual sensors that can send data wirelessly and a smartphone/tablet that will receive the wireless sensor data. Ultimately, we will also add a various feedback system to the RPDS so that users can acquire spatial information for excavation work and evaluate the efficacy of feedback. In addition, as we validated the current distance estimation method by manually placing the pipe and the sensor, this approach could have introduced some human error. In a future study, we will include distance measurement sensors such as ultrasonic sensors and an optical recording system that accurately obtain reference distances.

VI. Conclusion

We developed a custom-designed wireless sensor system with a specialized localization algorithm that eliminates the external magnetic interference and estimates the distance between the tip of the bucket of an excavator and a ferromagnetic pipe. We evaluated the system using the 14:1 lab-scaled excavator for accuracy of the distance estimation at eight distances from six pipes. Based on pre-collected data, we were able to find accurate linear regression models (higher than 0.95 of R^2) for all six pipes. We also applied the actual distance estimation during excavation movements at eight distances (from 5 to 75 mm, spaced 10 mm apart) using the linear regression models from the pre-collected data for validation. We were able to estimate the differences between the distances from the sensor to the pipe to be about 4.38±1.62mm for the six pipes at the eight distances in overall; when we estimated a target distance higher than 35 mm, the error rate was 7.77±3.68%. The preliminary study using the wireless sensor system with our localization algorithm shows significant potential for implementation on a real construction site to estimate the distance between an excavator and an underground pipe in real time. This system, which ultimately can be integrated with a sensory feedback modality, delivers distance information that will prevent excavation/drilling accidents on construction sites.

References

[1] L.O. Makana, N. Metje, I. Jefferson, M. Sackey, and C.D. Rogers, "Cost estimation of utility strikes: towards proactive management of street works," *Infrastructure Asset Management*, vol. 7, no. 2, pp.64-76. July 2018

[2] Common Ground Alliance, 2017 Damage Information Reporting Tool (DIRT) REPORT, 2018.

[3] A. Energy, Call 811 Before Excavating, (2019). Accessed: Nov. 7, 2021 [Online]. Available: https://www.atmosenergy.com/safety/call-811-excavating

[4] S. Li, H. Cai, and V.R. Kamat, "Uncertainty-aware geospatial system for mapping and visualizing underground utilities," *Automation in Construction*, vol. 53, pp. 105-19, May 2015.

[5] S. Li, H. Cai, and V.R. Kamat, "Integrating natural language processing and spatial reasoning for utility compliance checking," *Journal of Construction Engineering and Management,* vol. 142, no. 12, p. 04016074. Dec. 2016.

[6] S. Talmaki, and V.R. Kamat, "Real-time hybrid virtuality for prevention of excavation related utility strikes," *Journal of Computing in Civil Engineering,* vol. 28, no. 3, p.04014001, May 2014.

[7] S.W. Jaw, R. Van Son, V.K.H. Soon, G. Schrotter, R.L.W. Kiah, S.T.S. Ni, and J. Yan, "The Need for a Reliable Map of Utility Networks for Planning Underground Spaces," in 17th IEEE Int. Conf. Ground Penetrating Radar (GPR) 2018, June 2018, pp. 1-6.

[8] C. Plati, and X. Dérobert, "Inspection Procedures for Effective GPR Sensing and Mapping of Underground Utilities and Voids, with a Focus to Urban Areas," *in Civil engineering applications of ground penetrating radar*, Springer, Cham, 2015, pp. 125–145.

[9] S. Jazayeri, A. Saghafi, S. Esmaeili, C.P. Tsokos, "Automatic object detection using dynamic time warping on ground penetrating radar signals," *Expert Syst. Appl*. vol. 122, pp. 102–107, May 2019.

[10] A. Atef, H. Harbi, amd M. Rashed, "Adaptive boxcar background filtering for real-time GPR utility detection," *Arab. J. Geosci.*, vol. 11, no. 1, pp. 1-9, Jan. 2018.

[11] C. Yuan, S. Li, H. Cai, and V.R. Kamat, "GPR Signature Detection and Decomposition for Mapping Buried Utilities with Complex Spatial

Configuration," *J. Comput. Civ. Eng.* vol. 32, no. 4, p. 4018026. July 2018.

[12] P.G. Tabarro, J. Pouliot, L.M. Losier, and R. Fortier, "Detection and Location of Buried Infrastructures Using Ground Penetrating Radar: A New Approach Based on GIS and Data Integration," *Int. J. 3-D Inf. Model.,* vol. 7, no. 2, pp. 57-77, Apr. 2018.

[13] X. Zhou, H. Chen, J. Li, "Mapping the buried pipelines from GPR and GPS data," *in 2nd Int. Conf. Softw. Eng. Inf. Manag. (ICSIM 2019), Association for Computing Machinery*, Bali Indonesia, 2019, pp. 199–203.

[14] J. Cai, S. Li, H. Cai, "Accurate mapping of underground utilities: An information fusion approach based on dempster-shafer theory," *in Construction Research Congress 2018*, pp. 712– 721.

[15] J. Yan, S.W. Jaw, R. Van Son, K.H. Soon, G. Schrotter, "Three-dimensional data modelling for underground utility network mapping," Remote Sensing and Spatial Information Sciences, vol. 42, no. 4, pp.711-715, 2018.

[16] E. Skartados, I. Kostavelis, D. Giakoumis, A. Simi, G. Manacorda, D. Ioannidis, D. Tzovaras, Ground Penetrating Radar Image Processing Towards Underground Utilities Detection for Robotic Applications, *in 2018 IEEE Intl. Conff on Control, Artificial Intelligence, Robotics & Optimization (ICCAIRO),* May 2018, pp. 27-31.

[17] Common Ground Alliance, Call811, (2020). Accessed: Nov. 7, 2021 [Online]. Available: http://call811.com/

[18] A.J. Al-Bayati, L. Panzer, and A. Karakhan, "Reducing Damages to Underground Infrastructure: Performance Evaluation of One-Call Notification Program," *Pract. Period. Struct. Des. Constr.* vol. 24, no. 4, p. 4019018, Nov. 2019.

[19] Spear, J.E. Preventing Damage to Underground Utilities, Water Well J. (2016). Accessed: Nov. 7, 2021 [Online]. Available: https://waterwelljournal.com/preventing-damage-underground-utilities/

[20] PHMSA, Significant Incidents Listing, U.S. Dep. Transp. (2010). Accessed: Nov. 7, 2021 [Online]. Available: https://primis.phmsa.dot.gov/comm/reports/safety/IncDetYr_syr_2010_eyr_2010_flt_sig_cause_ALL-OTHER-CAUSES.html

[21] W.A. Tanoli, A. Sharafat, J. Park, and J.W. Seo, "Damage Prevention for underground utilities using machine guidance," *Autom. In Constr.* vol. 107, p. 102893. Nov. 2019.

[22] S. Ortega, J. Wendel, J. Santana, S. Murshed, I. Boates, A. Trujillo, A. Nichersu, and J. Suárez, "Making the Invisible Visible—Strategies for Visualizing Underground Infrastructures in Immersive Environments," *ISPRS Int. J. Geo-Information*, vol. 8, no. 3, p. 152, Mar. 2019.

[23] L.L. olde Scholtenhuis, X. den Duijn, and S. Zlatanova, "Representing geographical uncertainties of utility location data in 3D," *Autom. In Constr.*, vol. 96, pp. 483–493. Dec. 2018.

[24] A. Fenais, N. Smilovsky, and S.T. Ariaratnam, "Using Augmented Reality in Horizontal Directional Drilling to Reduce the Risk of Utility Damages," *in: Pipelines 2018 Util. Eng. Surv. Multidiscip. Top. - Proc. Sess. Pipelines 2018 Conf., American Society of Civil Engineers (ASCE),* Jul. 2018, pp. 290–298.

[25] S. Talmaki, V.R. Kamat, and H. Cai, "Geometric modeling of geospatial data for visualization-assisted excavation," *Adv. Eng. Informatics,* vol. 27, no. 2, pp. 283–298, Apr. 2013.

[26] X. Su, S. Talmaki, H. Cai, and V.R. Kamat, "Uncertainty-aware visualization and proximity monitoring in urban excavation: a geospatial augmented reality approach," *Vis. in Eng.,* vol. 1, no. 1, pp. 1–13, Dec. 2013.

[27] J.S. Lee, Y. Ham, H. Park H, J. Kim, "Challenges, tasks, and opportunities in teleoperation of excavator toward human-in-the-loop construction automation," *Automation in Construction*, vol.135, pp. 104119, Mar. 2022.

[28] S. Hwang and J. Song, "Monocular vision-based SLAM in indoor environment using corner, lamp, and door features from upward-looking camera," *IEEE Trans. Ind. Electron.,* vol. 58, no. 10, pp. 4804–4812, Oct. 2011.

[29] R. C. Luo and C. C. Lai, "Enriched indoor map construction based on multisensor fusion approach for intelligent service robot," *IEEE Trans. Ind. Electron.,* vol. 59, no. 8, pp. 3135–3145, Aug. 2012.

[30] H. Alismail, L. D. Baker, and B. Browning, "Continuous trajectory estimation for 3D SLAM from actuated LIDAR," *in Proc. IEEE Int. Conf. Robot. Autom.,* 2014, pp. 6096–6101.

[31] B. Wu, and C. Jen, "Particle-filter-based radio localization for mobile robots in the environments with low-density WLAN APs," *IEEE Trans. Ind. Electron.,* vol. 61, no. 12, pp. 6860–6870, Dec. 2014.

[32] K. Choi, W. Ra, and S. Park, "Robust least squares approach to passive target localization using ultrasonic receiver array*," IEEE Trans. Ind. Electron.,* vol. 61, no. 4, pp. 1993–2002, Apr. 2014.

[33] B. Li, J. Lu, W. Xiao, and T. Lin, "In-field fast calibration of FOG-based MWD IMU for horizontal drilling," *Meas. Sci. Technol.,* vol. 26, no. 3, p. 035001, Jan. 2015.

[34] Y. Zhang, Y. Wang, T. Yang, R. Yin, and J. Fang, "Dynamic angular velocity modeling and error compensation of one-fiber fiber optic gyroscope (OFFOG) in the whole temperature range," *Meas. Sci. Technol.,* vol. 23, no. 2, p. 025101, Jan. 2012,

[35] Z. Yanbo, S. Xiaofeng, Z. Huihui, and Z. Jun, "Dynamical measurement of drill tool attitude at stick-slip and continuous rotation mode in vertical drilling," *in Proc. 6th IEEE Conf. Ind. Electron. Appl.,* 2011, pp. 2698–2701.

[36] M. Elgizawy, A.M. Noureldin, and N. El-Sheimy, "MEMS gyroscope while-drilling environment qualification testing," in *Proc. IADC/SPE Drilling Conf. Exhib., 201*0, pp. 1-14.

[37] Z. Wang, M. Poscente, D. Filip, and M. Dimanchev, "Rotary in-drilling alignment using an autonomous MEMS-based inertial measurement unit for measurement-while-drilling processes," *IEEE Instrum. Meas. Mag.,* vol. 16, no. 6, pp. 26–34, Dec. 2013.

[38] Z. Yanshun, W. Shuwei, and F. Jiancheng, "Measurement-while-drilling instrument based on predigested inertial measurement unit," *Trans. Instrum. Meas.,* vol. 61, no. 12, pp. 3295–3302, Aug. 2012.

[39] C. Mullins, "Magnetic susceptibility of the soil and its significance in soil science—A review," *J. Soil Sci.,* vol. 28, no. 2, pp. 223–246, Jun. 1977.

[40] J. Priest, T. Quinn, and E. Frost, Jr., "Magnetic interference effects on accelerometer and magnetometer data: Detection, quality control and correction," *in Proc. SPWLA 55th Annu. Logging Symp*., May 2014, pp.1-13.

[41] T. Liu and B. Wang, "Guidance method in HDD based on rotating magnetic field," *IEEE Trans. Geosci. Remote Sens.,* vol. 52, no. 1, pp. 71–75, Mar. 2014.

[42] J. Vcelak, P. Ripka, and A. Zikmund, "Long-range magnetic tracking system," *IEEE Sensors J.,* vol. 15, no. 1, pp. 491–496, Aug. 2015.

[43] B. Park and H. Myung, "Underground localization using dual magnetic field sequence measurement and pose graph SLAM for directional drilling," *Meas. Sci. Technol.,* vol. 25, no. 12, p 125101, Oct. 2014.

[44] B. Park, and H. Myung, "Resilient underground localization using magnetic field anomalies for drilling environment," *IEEE Trans. Ind. Electron.,* vol. 65, no. 2, pp. 1377-1387, July 2017.

[45] Z.Y. Guo, D.J. Liu, Q. Pan, and Y.Y. Zhang, "Forward modeling of total magnetic anomaly over a pseudo-2D underground ferromagnetic pipeline," *Journal of Applied Geophysics*, vol. 113, pp.14-30, Feb. 2015.

[46] P. Wu, and Z. Guo, "High-precision inversion of buried depth inurban underground iron pipelines based on AM-PSO algorithm for magnetic anomaly" *Progress In Electromagnetics Research C*, vol. 100, pp.17-30. 2020.

[47] C. Wan, M. Pan, Q. Zhang, F. Wu, L. Pan, and X. Sun, "Magnetic anomaly detection based on stochastic resonance," *Sensors and Actuators A: Physical* vol. 278, pp. 11–17, Aug. 2018.

[48] T. Sun, X. Wang, J. Wang, X. Yang, T. Meng, Y. Shuai, and Y. Chen, "Magnetic anomaly detection of adjacent parallel pipelines using deep learning neural networks," *Computers & Geosciences*, vol. 159, p. 104987, 2022

[49] S. Feng, D. Liu, X. Cheng, H. Fang, and C. Li, "A new segmentation strategy for processing magnetic anomaly detection data of shallow depth ferromagnetic pipeline," *J. Appl. Geophys*. vol. 139, pp. 65–72, Apr. 2017.

[50] Z. Guo, D. Liu, Q. Pan, Y. Zhang, Y. Li, and Z. Wang, "Vertical magnetic field and its analytic signal applicability in oil field underground pipeline detection," *J. of Geophysics and Engineering*, vol. 12, no. 3, pp. 340-350, June 2015.

[51] Q. Pan, D.J. Liu, Z.Y. Guo, H.F. Fang, and M.Q. Feng, "Magnetic anomaly inversion using magnetic dipole reconstruction based on the pipeline section segmentation method," *J. of Geophysics and Engineering*, vol. 13, no. 3, pp. 242-258, June 2016.

[52] A. Sheinker, L. Frumkis, B. Ginzburg, N. Salomonski, and B.Z. Kaplan, "Magnetic anomaly detection using a three-axis magnetometer," *IEEE Trans. Magn*. vol. 45, no. 1, pp. 160–167. Feb. 2009.

[53] A. Sheinker, and M.B. Moldwin, "Magnetic anomaly detection (MAD) of ferromagnetic pipelines using principal component analysis (PCA)," *Meas. Sci. Technol.* vol. 27, no. 4, p. 45104, Mar. 2016.

[54] Z. Zhao, M. Yeo, S. Manoharan, S.C. Ryu, H. Park, "Electrically-Evoked proximity Sensation can enhance fine finger control in telerobotic pinch," *Scientific reports*, vol. 10, no. 1, pp. 1-12, Jan. 2020.
[55] D. Dollahon, S. Ryu, H. Park, "Pinching Force Changes by Modulating the Interaction Gain over the Fingertip," *IEEE Access*, vol. 10, pp. 9744-49, Jan. 2022.
[56] X. Huo, J. Wang, and M. Ghovanloo, "A magneto-inductive sensor based wireless tongue-computer interface," *IEEE Trans. Neural Syst. Rehabil. Eng.* vol. 16, no. 5, pp. 497–504. Aug. 2008.
[57] J. Kim, H. Park, M. Ghovanloo, et al., "The tongue enables computer and wheelchair control for people with spinal cord injury," *Science translational medicine*, vol. 5, no. 213, pp.213ra166-213ra166, 2013.
[58] J. Kim, H. Park, M. Ghovanloo, et al., "Assessment of the tongue-drive system using a computer, a smartphone, and a powered-wheelchair by people with tetraplegia," *IEEE Transactions on Neural Systems and Rehabilitation Engineering*, vol. 24, no. 1, pp. 68-78, 2016.
[59] H. Park, M. Kiani, H.M. Lee, J. Kim, J. Block, B. Gosselin, and M. Ghovanloo, "A wireless magnetoresistive sensing system for an intraoral tongue-computer interface," IEEE transactions on biomedical circuits and systems, vol. 6, no. 6, pp. 571-585, 2012.
[60] J. Kim, X. Huo, J. Minocha, J. Holbrook, A. Laumann, and M. Ghovanloo, "Evaluation of a smartphone platform as a wireless interface between tongue drive system and electric-powered wheelchairs," *IEEE transactions on biomedical engineering*, vol. 59, no. 6, pp. 1787-1796, 2012.
[61] BNO055, Accessed: Nov. 7, 2021 [Online]. Available: https://www.bosch-sensortec.com/products/smart-sensors/bno055/
[62] A. Cohen, Biomedical Signal Processing, CRC Press, 1986.
[63] F.L. Litvin, A. Fuentes, Gear Geometry and Applied Theory SECOND EDITION, 2nd ed., Cambridge University Press, New York, 2004.

Jeonghee Kim (S'10–M'18) was born in Daegu, South Korea. She received the B.S. degrees in electrical engineering from Kyungpook National University, Daegu, South Korea, and the University of Texas at Dallas, Richardson, TX in 2007 and 2008, respectively, and the M.S. degree in electrical engineering and computer science at the University of Michigan, Ann Arbor, MI in 2009. She received her doctoral degree supervised by Dr. Stephen P. DeWeerth and Dr. Omer T. Inan in School of Electrical and Computer Engineering at Georgia Institute of Technology, Atlanta, GA in 2018.

She is currently an assistant professor in the department of Engineering Technology and Industrial Distribution at Texas A&M University, College Station, TX and a director of the Quantitative Neuro Rehabilitation Lab since 2018.

Youngjib Ham was born in Gangneung, South Korea. He received the B.S. degree in Rural Systems Engineering, and M.S. degree in Architectural Engineering from Seoul National University, Seoul, South Korea in 2009 and 2011, rexpectively. He received the M.S. degree in Computer Science, and the Ph.D. in Civil Engineering from University of Illinois at Urbana Champaign, Urbana, IL in 2014 and 2015, respectively.

He is currently a history maker homes endowed associate professor in the depratment of construction sceicne and a director of smart construction, smart city, and smart building research lab at Texas A&M University. He is also a research affiliate at Texas A&M Institute of Data Science, a faculty fellow at Hazard Reduction and Recovery Center, and an affiliate at Texas A&M Transportation Institute.

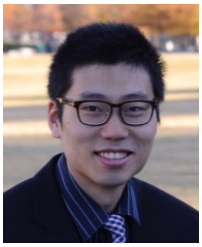

Hangue Park (S'10–M'17) was born in 1980. He received both the B.S. and M.S. degrees from Seoul National University, Seoul, Korea, in 2006 and 2008, respectively. He received his doctoral degree supervised by Dr. Stephen P. DeWeerth and Dr. Boris Prilutsky in School of Electrical and Computer Engineering at Georgia Institute of Technology, Atlanta, GA in 2018.

He is an assistant professor in ECE at Texas A&M University and the principal investigator of the INPL. He is also a research faculty at Texas A&M Institute for Neuroscience and The Texas Brain and Spine Institute, and a TIRR Foundation Fellow at The Institute for Rehabilitation and Research Foundation.